

An Elaboration on Order-Adaptive Regularisation for Variational Optical Flow: Global, Local and in Between

Hauptseminar Recent Advances in Computer Vision

David Hägele

Abstract—In variational optic flow estimation, the flow field between two consecutive images of a sequence is estimated by minimizing an energy functional. Usually this functional uses a regularization term in order to avoid unreasonable kinds of flow fields and allow for a unique solution to the ill-posed problem. Often the regularization is formulated as a constraint in terms of vanishing flow derivative of either first or second order which makes an algorithm suitable for different kinds of motion to be estimated.

This paper discusses the recent approach by Maurer et al. on adaptively selecting regularization order to allow for a flexible method that can solve typical first and second order flow problems equally well. This approach also overcomes framewise exclusive regularization order, which is desireable as fronto-parallel and affine motions may be present at the same time.

1 INTRODUCTION

In computer vision, the field of optic flow deals with the estimation of a 2-dimensional flow field based on two consecutive frames of an image sequence. This is useful for the detection and tracking of objects, e.g. in robotics [14], or in video compression tasks [9]. Different methods for flow estimation exist, Barron et al. classified the different approaches into differential, matching, energy-based and phase-based methods [2]. The differential methods are more commonly known as variational methods as they rely on the calculus of variations. Typically variational models use an energy functional consisting of a data term and a regularization term which are to be minimized. The regularization term is used to overcome ambiguous solutions to the optic flow problem by placing constraints on the flow field. Commonly the regularization terms are either of first or second order which allows for different kinds of flow fields to evolve. In the following the concept of variational flow estimation is recapitulated and the variational approach by Maurer, Stoll and Bruhn [10], which allows for adapting regularization order, is motivated and presented.

2 VARIATIONAL OPTIC FLOW

In this section the general framework for flow estimation using variational methods is recapitulated.

Given two subsequent images of an image sequence

$$I_0, I_1 : \Omega \subset \mathbb{R}^2 \rightarrow \mathbb{R}^2,$$

we seek the displacement vector field

$$\vec{u} = (u \ v)^\top : \Omega \subset \mathbb{R}^2 \rightarrow \mathbb{R}^2$$

that maps I_0 onto I_1 such that

$$I_0(\vec{x}) = I_1(\vec{x} + \vec{u}(\vec{x})).$$

To estimate the flow function \vec{u} an energy functional is minimized. Typically this functional consists of two terms, a data term $D(\vec{u})$ and a regularization term $R(\vec{u})$.

$$\vec{u}' = \underset{\vec{u}}{\operatorname{argmin}} E(\vec{u})$$

$$E(\vec{u}) = D(\vec{u}) + \alpha R(\vec{u})$$

In this framework, the data term is used to penalize flow functions which violate certain constancy assumptions on image features, such as the brightness constancy assumption.

$$D_{\text{bright}}(\vec{u}) = \int_{\Omega} (I_0(\vec{x}) - I_1(\vec{x} + \vec{u}(\vec{x})))^2 d\vec{x}$$

As the data term is insufficient for solving this problem and would yield multiple ambiguous solutions as illustrated in fig. 1, the regularization term is used to overcome this inconvenience and penalize flow functions that are unlikely. This is done by setting up constraints for the flow, such as the first order smoothness assumption.

$$R_{\text{smooth}}(\vec{u}) = \int_{\Omega} ||\nabla u||_2^2 + ||\nabla v||_2^2 d\vec{x}$$

This assumption enforces constant flow due to penalizing non vanishing gradients, which amount to changes in the vector field.

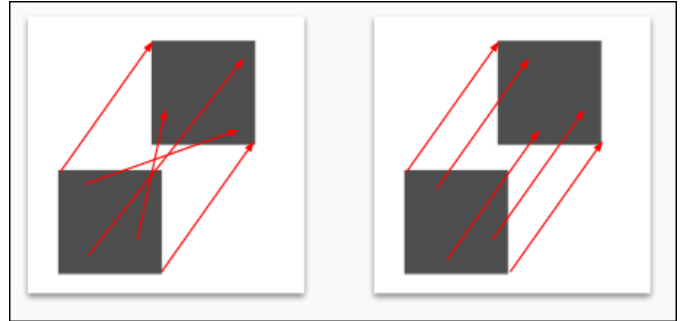


Figure 1: Images show a rectangle that moved from bottom left to top right. The red arrows sketch a flow field explaining where the pixels moved. Even though both fields perfectly fulfill a data term with brightness and gradient constancy assumption, only the right field is reasonable and would minimize a first order smoothness regularization.

In order to minimize the energy functional, an iterative update scheme is developed using the Euler-Lagrange equation [15].

3 MOTIVATION

As explained in section 2 the regularization term can be used to constrain the “type” of the estimated flow function. In practice either first or second order smoothness assumptions are made in which a flow function minimizes the regularization term when its first or second derivative vanishes. Therefore, first order methods are suitable for motion that is constant, i.e. parallel to the image plane. Second order methods can be leveraged for estimating affine flow fields as the class of linear functions implies vanishing second derivative. Figure 2 shows a constant and linear flow field for comparison.

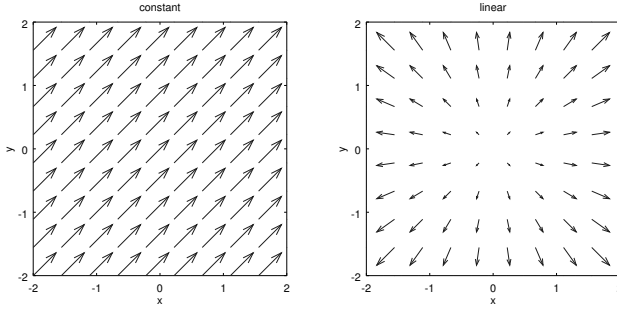


Figure 2: Graphs show vector fields of different behaviour, left is constant with $f(x,y) = (1 \ 1)^\top$, right is linear with $f(x,y) = (x \ y)^\top$. Constant flow is typical for motion parallel to the image plane, linear flow for motion orthogonal to the image plane.

Depending on the situation in the image sequence, a constant flow field may be more reasonable than a linear one. Imagine for example a sequence captured from the view point of a car driver who waits at a crossing while other cars pass the crossing from left to right in front of him. The optic flow in this situation would be constant as all cars move in the same direction parallel to the image plane. Now imagine the car driver moving forwards as the crossing is now free, the whole scene around him will appear to move towards him. The optic flow is now linear as the surroundings move perpendicular to the image plane. However, the flow behaviour is not exclusive, both constant and linear flow can be present in the same sequence, for example when another car heading in the same direction switches lanes. To account for such situations, a variational model has to make more sophisticated assumptions than simple first or second order smoothness.

Fortunately, the presented approach manages to combine first and second order regularisation and even adaptively choose optimal order for a given sequence. Moreover it provides different adaption schemes to enable a global, local, non-local and region based selection of regularisation.

4 VARIATIONAL MODEL

In this section the variational model by Maurer, Stoll and Bruhn introduced in their work [10] will be discussed in detail. As said in section 3 the variational model is able to adaptively choose regularization order. Therefore the regularisation term is a combination of a first and a second order part. First the models data term is discussed followed by the first and second order part of the regularization and their underlying concepts.

4.1 Dataterm

The employed data term in the variational model uses a combination of brightness and gradient constancy assumption.

$$D(\vec{u}) = \int_{\Omega} \psi_{\text{Ch}}(p_{\text{bright}}(\vec{u})) + \gamma \cdot \psi_{\text{Ch}}(p_{\text{grad}}(\vec{u})) d\vec{x} \quad (1)$$

$$p_{\text{bright}}(\vec{u}) = (I_1(\vec{x} + \vec{u}(\vec{x})) - I_0(\vec{x}))^2 \quad (2)$$

$$p_{\text{grad}}(\vec{u}) = \|\nabla I_1(\vec{x} + \vec{u}(\vec{x})) - \nabla I_0(\vec{x})\|_2^2 \quad (3)$$

In this setup, p_{bright} is the penalizer for the brightness constancy assumption and p_{grad} is the penalizer for the gradient constancy assumption which can be understood as a check for edges being mapped correctly. The parameter γ is used to weight the terms against each other. As can be seen p_{bright} and p_{grad} are quadratic penalizers, and are thus sensitive to outliers. To remove the strong influence of outliers on the minimization, the subquadratic charbonnier penalizer [5] ψ_{Ch} is used to robustify both constancy assumptions.

$$\psi_{\text{Ch}}(s^2) = 2\epsilon^2 \sqrt{1 + s^2/\epsilon^2} \quad (4)$$

Note that the charbonnier penalizer is a function of a squared argument so that an arbitrary quadratically penalized assumption can be plugged in. When plotting the function with respect to s instead of s^2 its behaviour becomes clearer, as shown in fig. 3. For values close to zero, the function penalizes quadratically and approaches linear behaviour in the limit $s \rightarrow \pm\infty$, resulting in outliers being less fatal.

4.2 First Order Regularizer

The first order term of the regularization is the anisotropic complementary regulariser by Zimmer et al. [16].

$$R_{1\text{st}}(\vec{u}) = \int_{\Omega} S_1(\vec{u}) d\vec{x} \quad (5)$$

$$S_1(\vec{u}) = \psi_{\text{PM}}((\vec{r}_1^\top \nabla u)^2 + (\vec{r}_1^\top \nabla v)^2) + \psi_{\text{Ch}}((\vec{r}_2^\top \nabla u)^2 + (\vec{r}_2^\top \nabla v)^2) \quad (6)$$

This term makes use of the eigenvectors of the regularisation tensor [16]. The regularization tensor is a generalization of the structure tensor [8] for arbitrary image features. In short, it summarizes gradient information within a neighborhood of a pixel. The eigenvector \vec{r}_1 points in the direction of steepest change (i.e. over an edge) while \vec{r}_2 is orthogonal to \vec{r}_1 (i.e. points along an edge).

Lets postpone the discussion of the regularization tensor for a second and get some intuition on the way S_1 works. As can be seen from eq. (6), the term uses two penalizer functions, the Charbonnier penalizer which was introduced in section 4.1 in eq. (4) and the Perona Malik penalizer ψ_{PM} [12].

$$\psi_{\text{PM}}(s^2) = \epsilon^2 \ln(1 + s^2/\epsilon^2) \quad (7)$$

As arguments to the penalizer functions, projections of the flow gradients onto the eigenvectors are used. These projections are minimal if the flow gradient vanishes as in standard first order smoothness terms. Special about this term are the different penalizations of projections on the first and second eigenvector respectively. The graphs of the two penalizer functions are shown in fig. 3, where it can be seen that values close to zero are penalized quadratically, values further away are penalized subquadratically in both functions. In the limit however, the Perona-Malik penalizer takes on smaller values than the charbonnier penalizer. This has the effect of flow changes tangent to the first eigenvector to be less costly than tangent to the second eigenvector. From the perspective of image features and the regularization tensor this is like getting a “discount” on flow change over an edge.

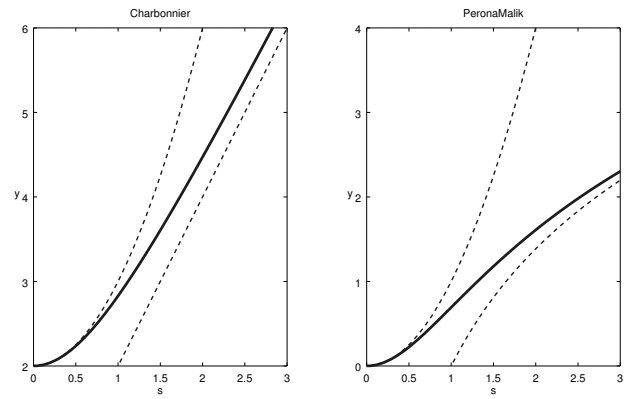


Figure 3: Graphs show penalizer functions and their asymptotic equivalents as dashed lines.

Left is charbonnier eq. (4) with $\epsilon = 1$ and asymptotic equivalents $\lim_{s \rightarrow 0} \psi_{\text{Ch}}(s^2) = s^2 + 2$ and $\lim_{s \rightarrow \infty} \psi_{\text{Ch}}(s^2) = 2s$.

Right is Perona Malik eq. (7) with $\epsilon = 1$ and asymptotic equivalents $\lim_{s \rightarrow 0} \psi_{\text{PM}}(s^2) = s^2$ and $\lim_{s \rightarrow \infty} \psi_{\text{PM}}(s^2) = 2 \ln(s)$.

4.2.1 Regularization Tensor

To continue the discussion of the regularization tensor, let's state its definition first.

$$S_{\Phi, \omega}(\vec{x}) = \int \omega(\tau) \begin{pmatrix} \Phi_x(\vec{x} - \tau)^2 & \Phi_x(\vec{x} - \tau)\Phi_y(\vec{x} - \tau) \\ \Phi_x(\vec{x} - \tau)\Phi_y(\vec{x} - \tau) & \Phi_y(\vec{x} - \tau)^2 \end{pmatrix} d\tau \quad (8)$$

$$S_{\Phi, \omega} = Q \Lambda Q^\top = (\vec{r}_1 \quad \vec{r}_2) \begin{pmatrix} \lambda_1 & 0 \\ 0 & \lambda_2 \end{pmatrix} \begin{pmatrix} \vec{r}_1^\top \\ \vec{r}_2^\top \end{pmatrix} \quad (9)$$

The tensor is a convolution of a weighting function ω with a matrix. The matrix is the outer product of the gradient of the selected image feature Φ which is calculated as $\nabla\Phi(\vec{x})\nabla\Phi(\vec{x})^\top$. For the structure tensor the image feature would be brightness $\Phi = I$, but as this is the generalization, Φ can be something else like the saturation value in HSV color space or luminance of CIE L*a*b*. Typically, the feature is chosen to be consistent with the feature used in the data term, which would be a combination of brightness and gradient norm. Using the eigendecomposition (eq. (9)), the orthonormal eigenvectors \vec{r}_1 and \vec{r}_2 are obtained which summarize the gradient distribution in the neighborhood defined by the weighting function ω . If the weighting function was a Dirac delta $\omega = \delta$ the eigendecomposition of the tensor would yield the normalized gradient as first eigenvector.

$$S_{\Phi, \delta} = \nabla\Phi\nabla\Phi^\top = \lambda_1 \cdot \vec{r}_1 \vec{r}_1^\top = (\vec{r}_1 \quad \vec{r}_2) \begin{pmatrix} \lambda_1 & 0 \\ 0 & 0 \end{pmatrix} \begin{pmatrix} \vec{r}_1^\top \\ \vec{r}_2^\top \end{pmatrix}$$

Here the first eigenvalue is the squared length of the gradient $\lambda_1 = |\nabla\Phi|^2$. Of course this discussion only holds for Dirac delta as weighting function, for others like Gaussian, the eigenvectors cannot be factored in this way.

4.3 Second Order Regularizer

The second order regularizer makes use of two auxiliary functions $\vec{a}(\vec{x})$ and $\vec{b}(\vec{x})$ which are connected to the flow \vec{u} using a coupling term S_2 . These auxiliary functions are as well unknown and are controlled by an auxiliary smoothness term S_{aux} .

$$R_{2\text{nd}}(\vec{u}) = \int_{\Omega} \inf_{\vec{a}, \vec{b}} [S_2(\vec{u}, \vec{a}, \vec{b}) + \beta \cdot S_{\text{aux}}(\vec{a}, \vec{b})] d\vec{x} \quad (10)$$

$$\begin{aligned} S_2(\vec{u}, \vec{a}, \vec{b}) &= \psi_{\text{PM}} \left((\vec{r}_1^\top (\nabla u - \vec{a}))^2 + (\vec{r}_1^\top (\nabla v - \vec{b}))^2 \right) \\ &\quad + \psi_{\text{Ch}} \left((\vec{r}_2^\top (\nabla u - \vec{a}))^2 + (\vec{r}_2^\top (\nabla v - \vec{b}))^2 \right) \end{aligned} \quad (11)$$

$$\begin{aligned} S_{\text{aux}}(\vec{a}, \vec{b}) &= \psi_{\text{PM}} \left(\sum_{k=1}^2 (\vec{r}_k^\top \mathcal{J}_{\vec{a}} \vec{r}_1)^2 + (\vec{r}_k^\top \mathcal{J}_{\vec{b}} \vec{r}_1)^2 \right) \\ &\quad + \psi_{\text{Ch}} \left(\sum_{k=1}^2 (\vec{r}_k^\top \mathcal{J}_{\vec{a}} \vec{r}_2)^2 + (\vec{r}_k^\top \mathcal{J}_{\vec{b}} \vec{r}_2)^2 \right) \end{aligned} \quad (12)$$

This regularization term can be interpreted as the integral over the infimal convolution of S_2 and S_{aux} with respect to the vector fields \vec{a} and \vec{b} .

The coupling term S_2 is similar to the first order term S_1 in that it uses the two penalizer functions ψ_{PM} and ψ_{Ch} to penalize non zero projections with respect to the eigenvectors of the structure tensor (eq. (8)). This time however, not the flow gradients themselves are projected, but the difference of the gradients to the auxiliary functions. The coupling term therefore becomes minimal if the gradients are equal to the auxiliary functions instead of equal to zero as in the first order term. Again, the projection on the first eigenvector is penalized less due to the behavior of the perona malik penalizer, but is not intuitive in the form written above. If instead we reformulate the projection as $(\vec{r}_1^\top (\nabla u - \vec{a}))^2 = (\vec{r}_1^\top \nabla u - \vec{r}_1^\top \vec{a})^2$ it becomes clear that the flow gradient and the auxiliary function are allowed to differ as long as they are roughly tangent to the first eigenvector.

In the auxiliary term S_{aux} the Jacobians of the auxiliary functions $\mathcal{J}_{\vec{a}}$ and $\mathcal{J}_{\vec{b}}$ are anisotropically penalized similar to the first order penalization of the flow gradients. Obviously, the auxiliary term is minimal

if the derivatives of the auxiliary functions vanish, allowing for constant auxiliary functions with changes at edges which are indicated by the regularization tensor. Due to the connection of the auxiliary functions to the flow gradients in the coupling term, the flow is indirectly constrained to be linear. This is because the nullspace of the second order term are functions with derivatives equal to the auxiliary functions which are constrained to be constant.

5 ORDER ADAPTION

In section 4, the data and regularization terms were discussed and it was explained that the first order regularizer enforces constant flow whereas the second order regularizer allows for linear flow. As illustrated in fig. 2 constant vector fields are suitable for modelling motion parallel to the image plane, motion orthogonal to the image plane can be modelled using a linear flow field. So what is needed to apply the most suitable regularizer depending on the current sequence, is an adaptive scheme. In the following four different schemes will be discussed, where the global scheme will be used to introduce the underlying concept of the schemes.

5.1 Global Scheme

The global adaptive scheme will be choosing order once for the whole image domain. To do so a general regularization term consisting of both, first and second order, will be extended. The general regularization term is a simple convex combination of the terms with weighting parameter $c \in [0, 1]$ and selection term $\phi_\lambda(c)$ of the following form.

$$\begin{aligned} R(\vec{u}, c) &= \int_{\Omega} \inf_{\vec{a}, \vec{b}} [c \cdot S_1(\vec{u}) + (1 - c) \cdot S_2(\vec{u}, \vec{a}, \vec{b}) \\ &\quad + \beta \cdot S_{\text{aux}}(\vec{a}, \vec{b}) + \phi_\lambda(c)] d\vec{x} \end{aligned} \quad (13)$$

It may be counter intuitive to only include S_1 and S_2 in the convex combination and not S_{aux} , but S_{aux} is independent of \vec{u} and merely used to constrain the auxiliary functions. S_1 and S_2 on the other hand are the energies with respect to the flow and are comparable to each other as they only differ in the projected quantity, which was already discussed in section 4.3. The goal thus, is to embed some information into the the weighting parameter c such that it equals to 1 when first order regularization has less energy than second order regularization and equals to 0 in the contrary case. However, since the class of linear functions which can be modelled using second order regularization includes constant functions, it is only desirable to use second order regularization when it yields a significant benefit over first order. To model this behaviour of c a sigmoid function of the benefit Δ of first over second order regularization is used as illustrated in fig. 4.

$$c = \frac{1}{1 + e^{-\Delta/\lambda}} \quad \text{with} \quad \Delta = T + \frac{1}{|\Omega|} \int_{\Omega} S_2 - S_1 d\vec{x} \quad (14)$$

Here λ is used to control the slope of the sigmoid function, and T is the threshold by which the second order regularizer has to be better than first order, so that second order will be used.

To get to this behavior of c from the euler lagrange equation's point of view, the corresponding selection term $\phi_\lambda(c)$ has to be found. By examining the regularizers partial derivative $\frac{\partial R}{\partial c} = 0$ we get to the following equation.

$$\begin{aligned} \frac{\partial R(\vec{u}, c)}{\partial c} &= \int_{\Omega} S_1(\vec{u}) - S_2(\vec{u}, \vec{a}, \vec{b}) + \phi'_\lambda(c) d\vec{x} = 0 \\ -\phi'_\lambda(c) \cdot |\Omega| &= \int_{\Omega} S_1(\vec{u}) - S_2(\vec{u}, \vec{a}, \vec{b}) d\vec{x} \\ \phi'_\lambda(c) &= \frac{1}{|\Omega|} \int_{\Omega} S_2(\vec{u}, \vec{a}, \vec{b}) - S_1(\vec{u}) d\vec{x} \end{aligned} \quad (15)$$

The right hand side of eq. (15) also occurs in eq. (14) which can be

reformulated as follows in order to be plugged in.

$$\begin{aligned} \frac{1}{|\Omega|} \int_{\Omega} S_2 - S_1 d\vec{x} &= \Delta - T \quad \text{with} \quad \Delta = -\lambda \cdot \ln\left(\frac{1}{c} - 1\right) \\ \phi'_\lambda(c) &= -\lambda \cdot \ln\left(\frac{1}{c} - 1\right) - T \end{aligned} \quad (16)$$

To obtain ϕ_λ we integrate both sides of eq. (16) and get the following selection term with integration constant C .

$$\phi_\lambda(c) = \lambda \left(\ln(1-c) - c \cdot \ln\left(\frac{1}{c} - 1\right) \right) - Tc + C \quad (17)$$

When choosing $C = T$ we can get a more intuitive formulation of the regularizer, using a cleverly tailored replacement ϕ for ϕ_λ .

$$\begin{aligned} \phi(c) &= \frac{\phi_\lambda(c) + T \cdot (c-1)}{\lambda} = \ln(1-c) - c \cdot \ln\left(\frac{1}{c} - 1\right) \quad (18) \\ &= c \cdot \ln(c) + (1-c) \cdot \ln(1-c) \end{aligned}$$

$$\begin{aligned} R(\vec{u}, c) &= \int_{\Omega} \inf_{\vec{a}, \vec{b}} [c \cdot S_1(\vec{u}) + (1-c) \cdot (S_2(\vec{u}, \vec{a}, \vec{b}) + T) \\ &\quad + \beta \cdot S_{\text{aux}}(\vec{a}, \vec{b}) + \lambda \cdot \phi(c)] d\vec{x} \end{aligned} \quad (19)$$

In this representation the threshold parameter T appears in the convex combination together with S_2 and can be interpreted as an extra cost to be paid in order to use second order regularization. The sigmoid slope parameter λ now works as a weight for the selection term ϕ which has become independent of λ . In fact the selection term has simplified quite a bit and it can be seen that it is a symmetric function which is illustrated in fig. 4. From the figure it can also be seen that ϕ is minimal for $c = \frac{1}{2}$ which can be interpreted as a prior on c for when the model is indecisive on regularization order. So by definition of ϕ neither of the regularizers is preferred, but due to the threshold T the decision is biased towards the first order regularization.

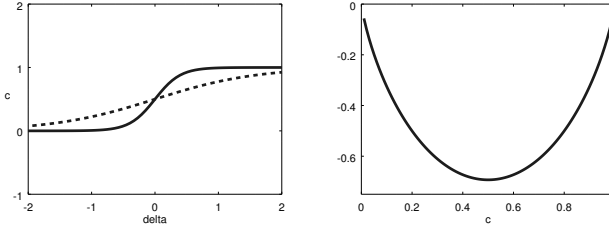


Figure 4: The left graph shows the weighting parameter c (eq. (14)) with respect to Δ , where Δ is the benefit of first over second order regularization biased by the threshold T . The solid line corresponds to $\lambda = 0.2$, the dotted line to $\lambda = 0.8$.

The right graph shows the selection term $\phi(c)$ (eq. (18)) which is axially symmetric to $c = \frac{1}{2}$.

5.2 Local Scheme

The previously introduced global scheme chooses regularization for the whole image domain, however, different parts of the scene may move differently so that it makes sense to allow for different regularization depending on the location. So instead of using a global weighting parameter c , it is replaced by a weighting function $c_{\text{local}}(\vec{x})$.

$$c_{\text{local}}(\vec{x}) = \frac{1}{1 + e^{-\Delta(\vec{x})/\lambda}} \quad \text{with} \quad \Delta(\vec{x}) = T + S_2 - S_1 \quad (20)$$

As a consequence Δ is now a spatially varying function as well, mapping to the benefit of first order regularization in a single pixel at \vec{x} , which allows the model to decide on order on a per pixel basis.

5.3 Non-Local Scheme

Since the local scheme allows for different regularization order per pixel based on a decision which only takes that pixels location into account, regularization order may fluctuate a lot in this model. To make the decision more consistent with the pixels neighborhood, the weighting function $c_{\text{local}}(\vec{x})$ is altered to take a rectangular shaped patch of pixels around it into account.

$$\bar{c}_{\text{nl}}(\vec{x}) = \frac{1}{|\mathcal{N}(\vec{x})|} \int_{\mathcal{N}(\vec{x})} c_{\text{nl}}(\vec{y}) d\vec{y} \quad (21)$$

$$\begin{aligned} R_{\text{nl}}(\vec{u}, c_{\text{nl}}) &= \int_{\Omega} \inf_{\vec{a}, \vec{b}} [\bar{c}_{\text{nl}} \cdot S_1(\vec{u}) + (1 - \bar{c}_{\text{nl}}) \cdot (S_2(\vec{u}, \vec{a}, \vec{b}) + T) \\ &\quad + \beta \cdot S_{\text{aux}}(\vec{a}, \vec{b}) + \lambda \cdot \phi(c_{\text{nl}})] d\vec{x} \end{aligned} \quad (22)$$

Here $\mathcal{N}(\vec{x})$ denotes the patch of \vec{x} and $|\mathcal{N}(\vec{x})|$ the patch size which is used for normalization. To find c_{nl} , $R_{\text{nl}}(\vec{u}, c_{\text{nl}})$ is minimized with respect to it and yields:

$$c_{\text{nl}}(\vec{y}) = \frac{1}{1 + e^{\Delta(\vec{y})/\lambda}} \quad \text{with} \quad \Delta(\vec{y}) = \int_{\mathcal{N}(\vec{y})} \frac{T + S_2 - S_1}{|\mathcal{N}(\vec{y})|} d\vec{x} \quad (23)$$

It may be surprising at first that the integrated c_{nl} itself contains a nested integral, but it is easy to convince yourself when thinking about a discrete version $c_{\vec{x}}$. When taking the derivative with respect to a single $c_{\vec{x}}$, then due to the integral in \bar{c}_{nl} we need to identify all terms which contain $c_{\vec{x}}$ (which is defined by the patch $\mathcal{N}(\vec{x})$). The reason for normalization $\frac{1}{|\mathcal{N}(\vec{x})|}$ being inside the integral is that patches at the boundaries vary in size (become smaller as less pixels are defined there).

5.4 Region-Based Scheme

The non-local scheme takes a neighborhood around a pixel into account for the decision on regularization order. To push it yet a little further, the region based scheme decides on order leveraging a level-set function $z(\vec{x}) : \Omega \rightarrow \mathbb{R}$ which divides the image space into first and second order regularized regions. Recall that a level-set function defines a closed curve (or curves) by $\{\vec{x} \mid z(\vec{x}) = 0\}$ that defines the decision boundary. The regions are thus defined by $\{\vec{x} \mid z(\vec{x}) < 0\}$ and $\{\vec{x} \mid z(\vec{x}) > 0\}$ which will be leveraged to regionally decide on regularization order. The corresponding regularizer reads as follows.

$$R(\vec{u}, z) = \int_{\Omega} c_{\text{rgn}}(z) \cdot S_1 + (1 - c_{\text{rgn}}(z)) \cdot (S_2 + T) + \theta \cdot |\nabla c_{\text{rgn}}(z)| d\vec{x} \quad (24)$$

$$c_{\text{rgn}}(z) = \frac{1}{1 + e^{z/\lambda}} \quad (25)$$

Here c_{rgn} is as well a sigmoid function, but chosen to approximate the heaviside function ($\lambda \rightarrow 0$) in order to obtain hard boundaries for the regions defined by z . The selection term from the previous schemes has been replaced by a smoothness term on c_{rgn} which penalizes non-smooth level set functions which results in less sign changes. Due to this penalization short paths for $\{\vec{x} \mid z(\vec{x}) = 0\}$ are favored resulting in smooth region boundaries.

Unfortunately this sophisticated scheme comes at a larger computational cost as z has to be evolved due to its smoothness term (compare [6]).

6 EXPERIMENTS

To evaluate this new approach, the authors conducted a few experiments which will be presented in this section.

To get an insight into the order selection of the algorithm with the different selection schemes, four synthetic image sequences were created from which the actual flow fields could be extracted as ground truth. Figure 5 shows the 4 image pairs and their corresponding flow fields.

By looking at the gradient magnitude $|\frac{\partial \vec{u}(\vec{x})}{\partial \vec{x}}|$ of the ground truth flow field, areas of vanishing gradients can be identified. Small values

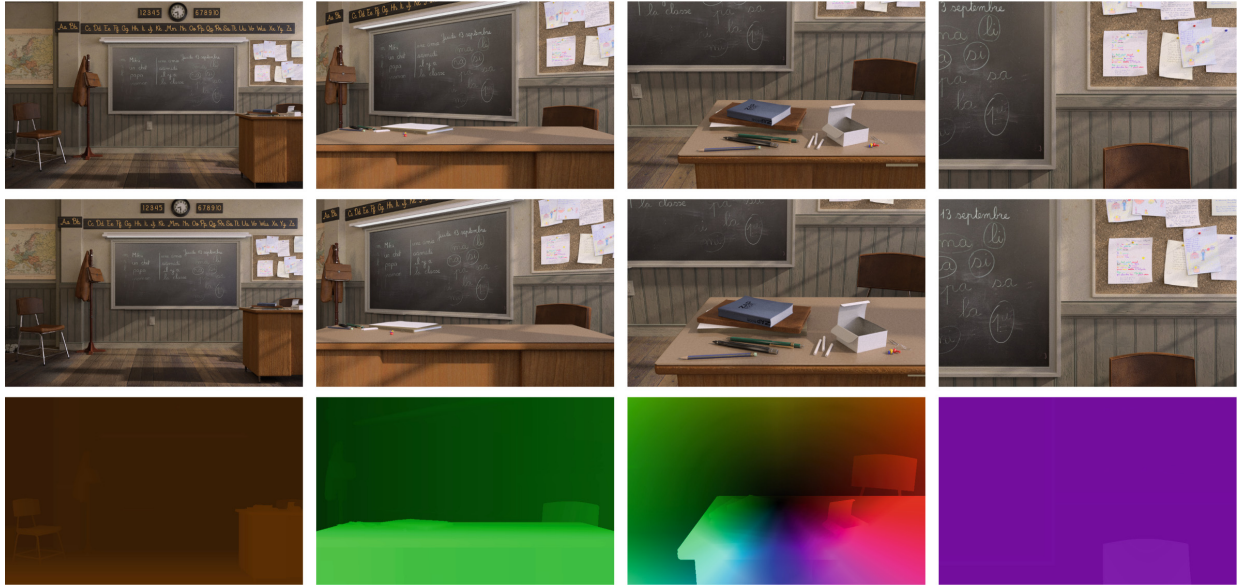


Figure 5: **Classroom sequences** [10]. First and second rows contains first frames and second frames. Third row contains the corresponding flow fields with flow direction encoded by hue, and flow magnitude by brightness. Each column corresponds to another sequence. Sequences 1,2 and 4 result from fronto-parallel motion as can be seen from the flow directions being the same for each pixel. Sequence 3 results from “fronto-orthogonal” or affine motion similar to the linear flow field depicted in fig. 2.

of the gradient magnitude thus indicate fronto-parallel motion whereas large values indicate affine motion. When these are compared to the order deciding c term of the different schemes, we can get a good impression on how the algorithm decided.

Figure 6 shows a comparison of the adaption behavior of the four different adaption schemes with respect to the ground truth gradient magnitude which works as an indicator for regularization order. For the global scheme (2nd row) the images are either completely white or completely black as the selection is global and thus the same for each pixel. For the global scheme, the algorithm surprisingly picked second order regularization for all sequences except for the fourth sequence. On the other hand, the fourth sequence has almost no depth to it and is thus truly fronto-parallel, so all schemes decided for first order for the majority of the pixels. What can also be seen is that for the local scheme (third row) the selection is pretty noisy, whereas the non-local and region based scheme show way more consistent order selection. Another insight is, that at motion discontinuities (i.e. edges) first order regularization is chosen predominately. Finally it is important to note that different order selection than indicated by the ground truth does not necessarily imply a bad result, since second order regularization contains first order as previously explained.

The quality of the approach has not only been assessed visually, but also quantitatively by evaluating the average end point error (AEE). The four regularizers (global, local, non-local, region) therefore were put up against a purely first and purely second order regularizer on the class room sequences. The second order regularizer used for comparison is an anisotropic variant of total generalized variation (TGV [3]) which also uses a coupling term and is not a purposefully chosen inferior regularizer. The AEE results for the different sequences are shown in table 1. From the table it can be seen that the best results are found in the order adaptive segment except for the fourth sequence where the first order regularizer shares first place with the adaptive local regularizer. Also the second order regularizer is already outperformed by the global order adaptive regularizer. For the rather fronto-parallel sequences, the local adaptive regularizer shines, but has really poor performance on the third sequence which is heavily affine in motion. The non-local and region order adaptive regularizers on the other hand, do quite well in all of the sequences, the region order adaptive however performs best on the affine motion sequence. Also note that the global order adaptive regularizer does not simply amount to choose

best out of first and second order, but instead relies on the same hyperparameters as the other adaptive regularizers (which were optimized jointly). Due to the number variables to be evolved in order to approximate the flow ($\vec{u}, \vec{a}, \vec{b}, c$) the runtimes of the adaptive regularizers are quite high compared to the simple first order regularizer which does not have a coupling term (and thus no auxiliary functions), especially the the region adaptive order regularizer takes quite a while as it involves the evolution of a smooth level set function.

Table 1: Average endpoint error - Classroom sequences [10]

regularization	Seq. 1	Seq. 2	Seq. 3	Seq. 4	runtime
first order	0.129	0.358	2.038	0.088	17s
second order	0.141	0.370	0.669	0.102	75s
adaptive global	0.141	0.365	0.667	0.095	100s
adaptive local	0.111	0.260	1.115	0.088	105s
adaptive non-local	0.116	0.275	0.737	0.095	120s
adaptive region	0.125	0.366	0.662	0.098	180s

Of course the results on the self made image sequences are not easily put into perspective with other recent approaches regarding optic flow, which is why the authors also put the regularizers up against the Middlebury benchmark [1], the Sintel benchmark [4] and the KITTI benchmarks of 2012 [7] and 2015 [11].

Table 2: Average endpoint error (AEE) and bad pixel error (BP) in four different benchmarks [10]

regularization	Middlebury (AEE)	Sintel (AEE)	KITTI '12 (BP)	KITTI '15 (BP)
first order	0.213	4.327	18.026	30.053
second order	0.222	6.518	9.461	22.736
adaptive global	0.211	4.213	9.423	22.424
adaptive local	0.211	4.082	11.537	24.938
adaptive non-local	0.211	4.145	9.468	22.158
adaptive region	0.208	4.358	9.415	22.343

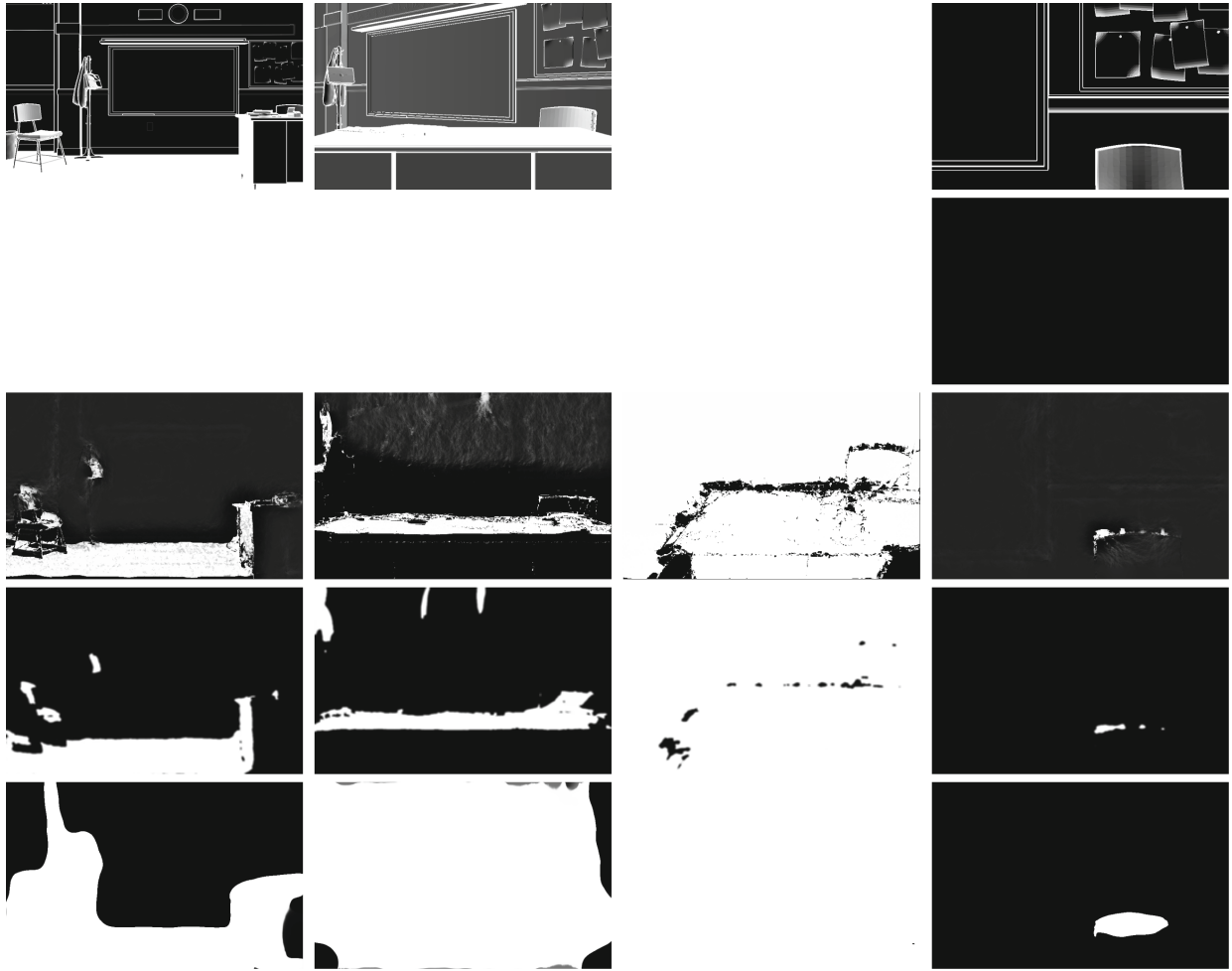


Figure 6: Adaption behavior of the different schemes [10]. Each column corresponds to the respective sequence introduced in fig. 5. First row shows the gradient magnitude of the ground truth flow fields, dark pixels indicate small magnitudes, bright pixels high magnitudes. The following rows correspond to the regularization order selection parameters c , dark pixels indicate first order regularization, bright pixels indicate second order regularization. The second row corresponds to the global scheme, third to local, fourth to non-local and fifth to region based.

The results obtained from these benchmark underline the findings from the experiments with the class room sequences. Again the non-local and region order adaptive regularizer perform pretty good overall. The local order adaptive regularizer scores high in the sintel benchmark yields rather poor results in the KITTI benchmarks where the simple second order and other adaptive regularizers worked quite well. So even on benchmark data, it can be seen that order adaption is worthwhile as it can provide better results than comparable single order approaches.

The authors decided on submitting the results of the non-local order adaptive regularizer to the respective benchmarks for comparison against other approaches of found in literature. It showed that the novel approach yields comparable or even better results than other first order approaches as for example Zimmer et al. [16] on the Sintel and Middlebury benchmarks. For the KITTI benchmarks the approach as well yields results that can compete with other second order approaches, like for example non-local total generalized variation (NLTGV) by Ranftl et al. [13].

7 CONCLUSION

In this paper, the approach to variational optic flow estimation by Maurer et al. [10] was explained. First the problem of exclusive first or second order regularization was explained, which is the suitability of the regularization order that is situation dependent. It was explained that first order regularization is well suited for fronto-parallel motion,

whereas second order works for affine motion.

The variational model of the novel approach was then introduced which uses a dataterm that combines a brightness and gradient constancy assumption and an order adaptive regularization term. The different parts of the regularization term were explained, which consists of an anisotropic first order part and anisotropic second order part that relies on the coupling of the gradients to two separate auxiliary functions.

Following that, the global adaptive scheme that selects order for the whole image domain was derived and three other adaptive schemes were shown (local, non-local, region based).

In the end, the novel regularizers were put to the test on synthetic sequences created by the authors which showed the adaption behavior of the four different schemes. The results of the regularizers on various benchmarks were presented as well. It showed that allowing for adaptively choosing regularization order is actually beneficial and yields a flexible variational model that performs well in both domains, that is fronto-parallel sequences and affine motion sequences.

REFERENCES

- [1] S. Baker, D. Scharstein, J. P. Lewis, S. Roth, M. J. Black, and R. Szeliski. A database and evaluation methodology for optical flow. *International Journal of Computer Vision*, 92(1):1–31, Mar 2011.
- [2] J. L. Barron, D. J. Fleet, and S. S. Beauchemin. Performance of optical flow techniques. *International Journal of Computer Vision*, 12(1):43–77, Feb 1994.

- [3] K. Bredies, K. Kunisch, and T. Pock. Total generalized variation. *SIAM Journal on Imaging Sciences*, 3(3):492–526, 2010.
- [4] D. J. Butler, J. Wulff, G. B. Stanley, and M. J. Black. A naturalistic open source movie for optical flow evaluation. In A. Fitzgibbon et al. (Eds.), editor, *European Conf. on Computer Vision (ECCV)*, Part IV, LNCS 7577, pages 611–625. Springer-Verlag, Oct. 2012.
- [5] P. Charbonnier, L. Blanc-Feraud, G. Aubert, and M. Barlaud. Deterministic edge-preserving regularization in computed imaging. *IEEE Transactions on Image Processing*, 6(2):298–311, Feb 1997.
- [6] D. Cremers and S. Soatto. Motion competition: A variational approach to piecewise parametric motion segmentation. *International Journal of Computer Vision*, 62(3):249–265, May 2005.
- [7] A. Geiger, P. Lenz, and R. Urtasun. Are we ready for autonomous driving? the kitti vision benchmark suite. In *Conference on Computer Vision and Pattern Recognition (CVPR)*, 2012.
- [8] D. Hafner, C. Schroers, and J. Weickert. Introducing maximal anisotropy into second order coupling models. In J. Gall, P. Gehler, and B. Leibe, editors, *Pattern Recognition*, pages 79–90, Cham, 2015. Springer International Publishing.
- [9] R. Krishnamurthy, P. Moulin, and J. Woods. Optical flow techniques applied to video coding. In *Proceedings., International Conference on Image Processing*, volume 1, pages 570–573 vol.1, Oct 1995.
- [10] D. Maurer, M. Stoll, and A. Bruhn. Order-adaptive regularisation for variational optical flow: Global, local and in between. In F. Lauze, Y. Dong, and A. B. Dahl, editors, *Scale Space and Variational Methods in Computer Vision*, pages 550–562, Cham, 2017. Springer International Publishing.
- [11] M. Menze and A. Geiger. Object scene flow for autonomous vehicles. In *Conference on Computer Vision and Pattern Recognition (CVPR)*, 2015.
- [12] P. Perona and J. Malik. Scale-space and edge detection using anisotropic diffusion. *IEEE Transactions on Pattern Analysis and Machine Intelligence*, 12(7):629–639, July 1990.
- [13] R. Ranftl, K. Bredies, and T. Pock. Non-local total generalized variation for optical flow estimation. In D. Fleet, T. Pajdla, B. Schiele, and T. Tuytelaars, editors, *Computer Vision – ECCV 2014*, pages 439–454, Cham, 2014. Springer International Publishing.
- [14] J. Serres and F. Ruffier. *Optic Flow-Based Robotics*, pages 1–14. American Cancer Society, 2016.
- [15] H. Weber and G. Arfken. *Essential Mathematical Methods for Physicists*, ISE, chapter 18 *Calculus of Variations*. Elsevier Science, 2003.
- [16] H. Zimmer, A. Bruhn, and J. Weickert. Optic flow in harmony. *International Journal of Computer Vision*, 93(3):368–388, Jul 2011.